J. metamorphic Geol., 1995, 13, 299–314

Deep crustal growth of quartz, kyanite and garnet into large-aperture, fluid-filled fractures, north-eastern Connecticut, USA

J. J. AGUE
Department of Geology and Geophysics, Yale University, PO Box 208109, New Haven, CT 06520-8109, USA

ABSTRACT A petrographic and petrological analysis of exceptionally well-preserved hydrothermal veins from the Merrimack synclinorium, north-eastern Connecticut, has been carried out in order to place new field-based constraints on fracture aperture dimensions and porosity in the lower continental crust. The veins preserve substantial open space today in outcrop, and contain mineral assemblages including subhedral to euhedral crystals of quartz, kyanite and almandine-rich garnet. Textural evidence indicates unequivocally that the vein minerals grew into macroscopic (mm- to cm-scale) open space between the vein walls. The veins are interpreted to have been large-aperture fractures along which significant advective fluid infiltration and chemical reaction occurred. The porosity of the rock mass due to open space between fracture walls today is *c.* 0.3%, but it could have been as large as several percent when the flow system was active. Quantitative thermobarometry results from vein mineral assemblages indicate that the fractures formed at pressures and corresponding crustal depths of *c.* 0.8 GPa and *c.* 30 km, and temperatures of 550–600° C. The depth of fracture formation corresponds to published estimates of the maximum burial depth of the Merrimack synclinorium during the Acadian orogeny. The formation of large-aperture fractures could increase significantly the transient permeability of the deep crust, and therefore influence metamorphic heat and mass transfer.

Key words: Connecticut, USA; deep crust; fluid flow; fractures; P–T path.

INTRODUCTION

The apertures and spacings of fractures directly influence critical rock properties including porosity and permeability (cf. Norton & Knapp, 1977; Walther & Orville, 1982; Walther, 1990; Manning & Bird, 1991; Hanson, 1992). Therefore, the physical characteristics of fracture systems will have a profound effect on the transport of heat and mass by metamorphic fluids. It is generally thought that fluid-filled fractures in the middle to lower continental crust have microscopic apertures ($<10^{-5}$ m), and that fracture porosity is vanishingly small (<0.1%). However, deep continental drilling results suggest that 'open' (macroscopic-aperture) fluid-filled fractures are present to depths of at least 11 km in continental crust (Kozlovsky, 1987). Furthermore, previous studies of exhumed metamorphic rocks indicate that macroscopic-aperture fractures may form at middle crustal levels in continental orogenic belts (*c.* 11–15 km; Oliver *et al.*, 1990, 1993), and even deeper levels in high-P, low-T subduction zone environments (e.g. Essene & Fyfe, 1967; Philippot & Selverstone, 1991). Although significant progress has been made in understanding fracture-controlled fluid flow in metamorphic rocks (cf. Rye *et al.*, 1976; Yardley, 1986; Chamberlain & Rumble, 1988; Walther, 1990), the upper limits on fracture aperture dimensions and fracture porosity in the deep parts of high-T continental orogenic belts are not well constrained. This is largely because fracture properties are obscured by deformation and recrystallization during orogenesis. Here I report on an exceptionally well-preserved metamorphic hydrothermal system in which high-P mineral assemblages grew into open (mm- to cm-scale aperture) fluid-filled fractures. The P–T conditions of hydrothermal mineral assemblage equilibration are estimated in order to place new constraints on the depths at which flow through large-aperture fractures can take place in high-T continental orogenic belts.

~~ague@milne.geology.yale.edu~~
JAY.AGUE@YALE.EDU

METHODS

Observations of vein–wallrock relations were made in the field, and on 58 rock specimens and 43 polished thin sections. Mineral compositions were determined using the JEOL JXA-8600 electron microprobe at Yale University in conjunction with natural and synthetic standards and off-peak background corrections. Five to 25 'spot' analyses of 1–4 crystals of each phase were done in each thin section. Average compositions of coexistng phases in mutual contact that were inferred on textural grounds to constitute hydrothermal parageneses are given in Tables 1–5. Backscattered electron images were also obtained using the Yale University

Table 1. Biotite analyses.

Type*	7 (i)	8-1 (iii)	9-1 (iii)	11a (i)	11b (i)	15-1 (iii)	18-sl (ii)	24-2 (ii)	25 (ii)
SiO_2	36.24	37.29	37.66	35.83	38.98	37.74	36.44	37.18	35.99
TiO_2	1.51	1.79	1.60	1.90	1.97	1.50	1.82	1.21	1.77
Al_2O_3	19.69	17.50	17.96	19.15	15.97	17.93	17.93	18.31	18.83
FeO	15.62	17.11	16.06	15.31	15.27	13.31	15.93	16.29	16.87
MnO	b.d.	0.03	0.04	0.03	0.06	b.d.	0.05	0.07	b.d.
MgO	13.69	14.32	14.71	14.04	14.82	15.38	14.00	14.11	13.25
BaO	0.42	0.11	0.02	0.87	0.13	b.d.	0.15	0.11	0.22
Na_2O	0.22	0.18	0.14	0.18	0.09	0.10	0.20	0.12	0.12
K_2O	8.96	9.06	9.25	8.98	8.72	8.89	9.04	9.05	9.31
F	0.35	0.79	0.60	0.33	0.46	0.35	0.53	0.35	0.23
Cl	0.13	0.24	0.18	0.16	0.40	0.24	0.20	0.22	0.22
Total	96.83	98.42	98.22	96.78	96.87	95.44	96.29	97.02	96.81
				Structural formula (11 O)					
Si	2.67	2.74	2.75	2.66	2.86	2.78	2.72	2.74	2.68
Al^{IV}	1.33	1.26	1.26	1.34	1.14	1.22	1.28	1.26	1.32
Al^{VI}	0.39	0.25	0.29	0.33	0.25	0.34	0.29	0.33	0.33
Ti	0.08	0.10	0.09	0.11	0.11	0.08	0.10	0.07	0.10
Fe	0.96	1.05	0.98	0.95	0.94	0.82	0.99	1.00	1.05
Mg	1.51	1.57	1.60	1.55	1.62	1.69	1.56	1.55	1.47
Σ	2.94	2.97	2.96	2.94	2.92	2.93	2.95	2.96	2.94
Ba	0.01	—	—	0.03	—	—	—	—	0.01
Na	0.03	0.03	0.02	0.03	0.01	0.01	0.03	0.02	0.02
K	0.84	0.85	0.86	0.85	0.82	0.84	0.86	0.85	0.88
F	0.08	0.18	0.14	0.08	0.11	0.08	0.13	0.08	0.05
Cl	0.02	0.03	0.02	0.02	0.05	0.03	0.03	0.03	0.03

* i, inclusion within garnet; ii, in contact with garnet rim in selvage; iii, in contact with garnet rim in open vein. b.d., below detection.

electron microprobe. Vein volume percents were estimated using 4–8-m-long measurement traverses across outcrops. Vein percent was computed as (total vein length)/(total vein + rock length). Fracture apertures along the traverses were measured perpendicular to fracture walls using a mm scale.

GEOLOGICAL SETTING

The field area, located in north-eastern Connecticut, is part of a highly deformed and metamorphosed sequence of

Table 2. Garnet analyses.

Type*	3-2 (i)	7 (i)	8-1 (iii)	9-1 (iii)	11a (i)	11b (i)	15-1 (iii)	18-sl (ii)	24-2 (ii)	25 (ii)	26-1 (ii)
SiO_2	37.67	37.97	37.20	37.07	37.42	38.25	37.91	37.45	37.19	37.20	38.25
TiO_2	0.10	0.03	0.02	0.03	0.03	0.12	0.04	0.03	0.05	0.10	0.14
Al_2O_3	21.48	21.31	21.24	21.01	21.20	21.57	21.43	21.24	21.30	21.12	21.54
FeO	29.89	31.50	32.46	33.68	30.75	29.11	33.64	33.52	32.98	32.52	30.62
MnO	1.30	1.39	1.71	1.61	1.85	2.40	1.67	1.54	1.88	1.93	1.13
MgO	4.37	3.73	3.76	3.55	3.72	4.16	3.58	3.66	3.28	3.23	3.98
CaO	5.49	4.98	3.26	3.07	5.15	5.33	2.82	2.80	3.66	3.83	5.52
Total	100.30	100.91	99.65	100.02	100.12	100.94	101.09	100.24	100.34	99.93	101.18
					Structural formula (12 O)						
Si	2.98	3.00	2.98	2.98	2.98	3.00	3.00	2.99	2.97	2.98	3.00
Ti	0.01	—	—	—	—	0.01	—	—	—	0.01	0.01
Al	2.00	1.98	2.01	1.99	1.99	1.99	2.00	2.00	2.01	2.00	1.99
Fe	1.97	2.08	2.18	2.26	2.05	1.91	2.23	2.24	2.21	2.18	2.01
Mn	0.09	0.09	0.12	0.11	0.13	0.16	0.11	0.10	0.13	0.13	0.08
Mg	0.51	0.44	0.45	0.43	0.44	0.49	0.42	0.44	0.39	0.39	0.47
Ca	0.47	0.42	0.28	0.26	0.44	0.45	0.24	0.24	0.31	0.33	0.46
X_{alm}	0.65	0.69	0.72	0.74	0.67	0.64	0.74	0.74	0.73	0.72	0.67
X_{sps}	0.03	0.03	0.04	0.04	0.04	0.05	0.04	0.04	0.04	0.04	0.03
X_{prp}	0.17	0.15	0.15	0.14	0.15	0.16	0.14	0.14	0.13	0.13	0.15
X_{grs}	0.15	0.14	0.09	0.09	0.14	0.15	0.08	0.08	0.10	0.11	0.15

* i, inclusion within garnet; ii, in contact with garnet rim in selvage; iii, in contact with garnet rim in open vein. b.d., below detection.

Table 3. Plagioclase analyses.

Type*	3-2 (i)	7 (i)	8-1 (iii)	9-1 (iii)	11a (i)	11b (i)	15-1 (iii)	18-sl (ii)	24-2 (ii)	25 (ii)	26-1 (ii)
SiO_2	60.24	61.59	57.73	57.31	60.60	62.08	59.85	60.01	59.29	58.28	58.23
Al_2O_3	25.00	24.50	26.98	27.51	24.93	24.09	25.61	25.34	26.69	26.85	26.43
FeO	0.29	n.a.	0.42	0.40	0.03	0.31	0.02	0.18	0.02	0.05	0.39
CaO	6.04	5.50	8.34	8.82	5.83	5.27	7.06	6.89	7.70	7.74	7.97
Na_2O	8.12	8.71	6.92	6.64	8.54	8.58	7.59	7.69	7.19	7.32	7.11
K_2O	0.02	0.07	0.03	0.06	0.07	0.08	0.08	0.08	0.06	0.05	0.07
Total	99.71	100.37	100.42	100.74	100.00	100.41	100.21	100.19	99.95	100.29	100.20
					Structural formula (8 O)						
Si	2.69	2.72	2.58	2.55	2.70	2.74	2.66	2.67	2.62	2.60	2.60
Al	1.32	1.28	1.42	1.45	1.31	1.26	1.34	1.33	1.39	1.41	1.39
Fe	0.01	—	0.02	0.02	—	0.01	—	0.01	—	—	0.02
Ca	0.29	0.26	0.40	0.42	0.28	0.25	0.34	0.33	0.37	0.37	0.38
Na	0.70	0.75	0.60	0.57	0.74	0.74	0.65	0.66	0.62	0.63	0.62
K	—	—	—	—	—	0.01	0.01	0.01	—	—	—
X_{an}	0.29	0.26	0.40	0.42	0.27	0.25	0.34	0.33	0.37	0.37	0.38
X_{ab}	0.71	0.74	0.60	0.58	0.72	0.74	0.66	0.67	0.63	0.63	0.62
X_{or}	—	—	—	—	—	0.01	0.01	0.01	—	—	—
ln(Ca/Na)	−0.89	−1.05	−0.41	−0.31	−0.98	−1.08	−0.67	−0.70	−0.52	−0.54	−0.48

* i, inclusion within garnet; ii, in contact with garnet rim in selvage; iii, in contact with garnet rim in open vein. b.d., below detection; n.a., not analysed.

Ordovician–Devonian sedimentary and igneous rocks known as the 'Merrimack synclinorium' (Figs 1 & 2; cf. Rodgers, 1981; Robinson & Tucker, 1982; Schumacher *et al.*, 1989). Deformation and metamorphism occurred during the Devonian Acadian orogeny. Throughout much of central Massachusetts and north-eastern Connecticut, metamorphic grade reached the granulite facies (Schumacher *et al.*, 1989; Thomson, 1992). Based on U–Pb ages of monazites from granulite facies rocks, Thomson *et al.* (1992) concluded that 'peak' thermal metamorphism occurred at 362–369 Ma. The synclinorium was apparently little affected by late Palaeozoic Alleghanian metamorphism and deformation (Gromet, 1989; Wintsch *et al.*, 1992).

Stratigraphic relations and the deformational history of

Table 4. Hornblende analyses.

Type*	3-2 (i)	11b (i)	26-1 (ii)
SiO_2	43.99	46.43	45.09
TiO_2	0.87	0.81	0.90
Al_2O_3	12.95	11.76	12.33
FeO	14.37	12.86	14.41
MnO	0.14	0.17	0.10
MgO	12.01	13.40	11.97
CaO	11.23	11.33	11.04
Na_2O	1.14	1.10	1.11
K_2O	0.65	0.37	0.57
F	0.12	0.18	0.12
Cl	0.38	0.13	0.23
Total	97.85	98.54	97.87
	Structural formula (23 O)		
Si	6.50	6.71	6.62
Al^{IV}	1.50	1.29	1.38
Al^{VI}	0.75	0.71	0.76
Ti	0.10	0.09	0.10
Fe	1.77	1.55	1.77
Mn	0.02	0.02	0.01
Mg	2.64	2.89	2.62
Ca	1.78	1.75	1.74
Na	0.33	0.31	0.32
K	0.12	0.07	0.11
F	0.06	0.08	0.06
Cl	0.10	0.03	0.06

* i, inclusion within garnet; ii, in contact with garnet rim in selvage; iii, in contact with garnet rim in open vein. b.d., below detection.

Table 5. Muscovite analyses.

Type*	7 (i)	25 (ii)
SiO_2	46.52	46.93
TiO_2	0.32	1.06
Al_2O_3	35.19	31.44
FeO	1.54	3.75
MnO	b.d.	b.d.
MgO	0.96	2.02
BaO	0.35	0.34
Na_2O	0.61	0.22
K_2O	9.72	9.63
F	0.02	0.10
Cl	0.02	0.20
Total	95.25	95.69
	Structural formula (11 O)	
Si	3.09	3.15
Al^{IV}	0.91	0.85
Al^{VI}	1.85	1.65
Ti	0.02	0.05
Fe	0.09	0.21
Mg	0.10	0.20
Σ	2.05	2.11
Ba	0.01	0.01
Na	0.08	0.03
K	0.83	0.83
F	—	0.02
Cl	—	0.02

* i, inclusion within garnet; ii, in contact with garnet rim in selvage; iii, in contact with garnet rim in open vein. b.d., below detection.

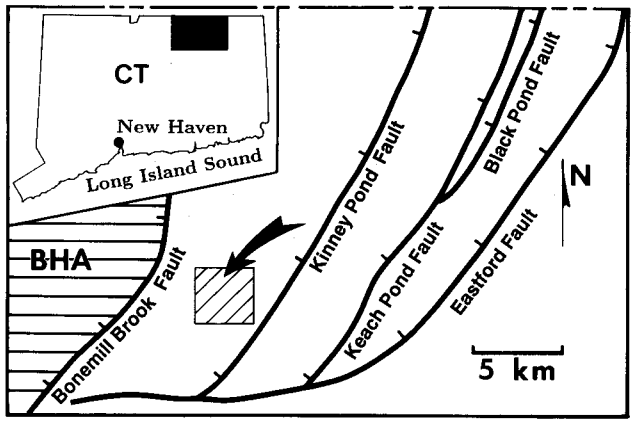

Fig. 1. Location of the Merrimack synclinorium (no ornament) and the Bronson Hill anticlinorium (BHA; horizontal rule) in north-eastern Connecticut, modified after Rodgers (1981). Map area is indicated by black box on inset Connecticut State map. Heavy lines are the major thrust faults discussed in detail by Rodgers (1981). Tick marks on hanging walls. Map area of Fig. 2 indicated by box with diagonal rule.

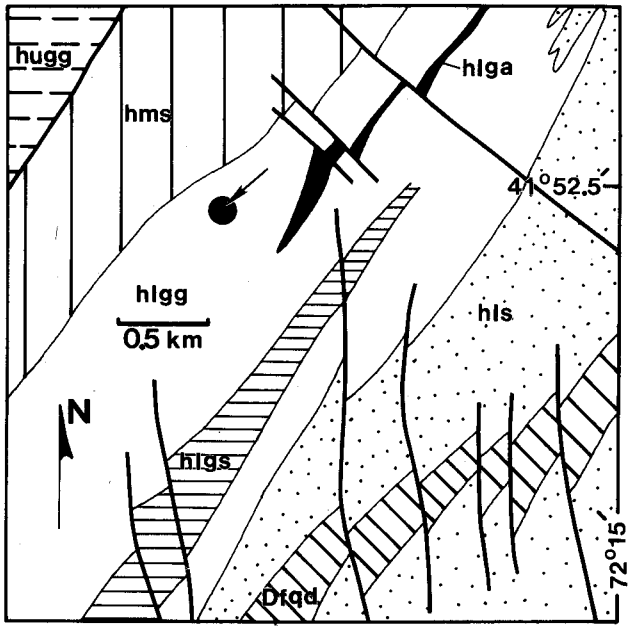

Fig. 2. Simplified map of geological relations in the vicinity of the vein locality, modified after Pease (1975), Peper & Pease (1975), Fahey & Pease (1977) and Rodgers (1985). Vein locality denoted by filled circle (with arrow). Stratigraphic nomenclature after Peper & Pease (1975). 'Peak' metamorphic grade is granulite facies. Metamorphic foliations strike NE–SW and dip *c.* 40° to *c.* 80° north-west throughout the map area. Thick lines denote faults. Peper & Pease (1975) concluded that most of the faults are normal faults, and that the intervening crustal blocks were displaced in a west-side-up sense. All rock units, except Dfqd, were assigned to the Hamilton Reservoir Formation (Devonian(?) to Ordovician(?)) by Peper & Pease (1975). hugg, Pl + Qtz + Bt gneiss with minor Di, Hbl and Grt; hms, Qtz + Pl ± Kfs ± Bt ± Grt ± Sil ± Crd gneiss and schist with minor graphitic and diopsodic gneiss; hlgg, Pl + Cpx + Opx + Bt ± Qtz ± Hbl ± Cum gneiss with minor intercalated ultramafic rock and sillimanite gneiss (see text); hlgs, sulphidic and graphitic sillimanite schist and gneiss; hlga, amphibolite; hls, Qtz + Pl + Kfs + Bt + Grt ± Sil gneiss and schist with minor quartzite and Pl + Qtz + Bt ± Grt gneiss; Dfqd, foliated quartz diorite (Devonian(?)). Minor Early Jurassic mafic dykes not shown. Mineral abbreviations after Kretz (1983).

the synclinorium are highly controversial. Peper & Pease (1976) and Rodgers (1981) proposed that the synclinorium is a roughly homoclinal sequence of west-dipping metasedimentary and meta-igneous rocks cut by a large number of throughgoing strike faults. According to Rodgers (1981), the faults are thrusts that are subparallel to the compositional layering and do not repeat any of the stratigraphic units. The faults are often marked by zones of mylonite or blastomylonite that formed at metamorphic grades slightly lower than 'peak' granulite facies conditions. In contrast, based on their studies of the same sequence of rocks in central Massachusetts, Robinson and co-workers (e.g. Field, 1975; Robinson, 1978; Robinson & Tucker, 1982) have argued that the synclinorium is a tightly folded stack of nappes which formed during three main stages of deformation. The first stage produced large, west-verging recumbent folds. In the second stage, the nappes were refolded back to the east such that their axial planes were rotated through the vertical to dip west. Robinson & Tucker (1982) concluded that most of the mylonites discussed by Rodgers (1981) formed during a third stage of deformation that was associated with the formation of gneiss domes to the west of the synclinorium.

Because of the major uncertainties which surround the stratigraphy and structural history of the Merrimack synclinorium, the tectonic setting in which orogenesis occurred remains unresolved. One of the most provocative tectonic interpretations was advanced by Rodgers (1981), who proposed that the synclinorium represents the deep roots of an accretionary prism that developed during late Ordovician to early Devonian subduction beneath the eastern North American continental margin. Rodgers (1981) inferred that the meta-igneous rocks of the Bronson Hill anticlinorium represent the corresponding magmatic arc (Fig. 1). Rodgers' (1981) model is consistent with many aspects of the regional geology, but it continues to be highly controversial (cf. Robinson & Tucker, 1982).

In spite of the debate over the tectonic history of the synclinorium, there is general agreement regarding its P–T path during Acadian orogenesis. The earliest phase of metamorphism appears to have been a low-P Buchan-style event which produced andalusite (now preserved as sillimanite pseudomorphs after andalusite) in pelites over a wide area within the synclinorium (e.g. Thomson *et al.*, 1992). As orogenesis continued, the rocks were further heated and compressed to 'peak' granulite facies conditions of 700–800° C and 0.5–0.7 GPa (cf. Schumacher *et al.*, 1989; Armstrong *et al.*, 1992). In terms of the three-stage deformation model advanced by Robinson and co-workers, the 'peak' metamorphism and synchronous regional deformation are inferred to post-date the nappe stage (e.g. Berry, 1992). Robinson & Tucker (1982) suggested that the metamorphism occurred during the stage of regional backfolding. Field relations and

quantitative thermobarometry indicate that mylonite formation took place as the synclinorium cooled into the amphibolite facies during continued compression at conditions of *c.* 0.8 GPa and 550–600° C (cf. Schumacher *et al.*, 1989; Armstrong *et al.*, 1992; Thomson *et al.*, 1992). To summarize, available evidence indicates that the region was metamorphosed along a broadly 'anticlockwise' P–T path.

VEIN–WALLROCK RELATIONS

Wallrocks

The veins are exposed over an area of *c.* 20 000 m^2, and are hosted by dark grey mafic gneiss which contains small amounts of intercalated pelitic gneiss and isolated pods and lenses of ultramafic gneiss (Figs 2 & 3a). Several different stratigraphic nomenclature systems have been used in the region; Pease (1975), Peper & Pease (1975) and Fahey & Pease (1977) mapped the gneiss as part of the 'Hamilton Reservoir Formation' (unit hlgg), whereas Rodgers (1985) referred to it as the 'gneiss member of the Brimfield schist'. Rock types in the vicinity of the field area are summarized in Fig. 2. The typical prograde assemblage in mafic gneiss is: plagioclase (*c.* An_{70-80}) + clinopyroxene + orthopyroxene + biotite ± quartz. The minerals are listed in the approximate order of decreasing abundance. The pelitic gneiss contains: orthoclase + plagioclase + biotite + garnet + sillimanite + cordierite ± spinel ± quartz. One pelitic gneiss sample contains sillilmanite pseudomorphs after andalusite, similar to those described from other localities in the Merrimack synclinorium (cf. Schumacher *et al.*, 1989; Thomson, 1992). The mineral assemblages in the gneisses indicate that 'peak' metamorphism took place at or near granulite facies conditions (cf. Turner, 1981), consistent with field relations elsewhere in the synclinorium. Variable retrograde alteration of pyroxenes to cummingtonite and rare hornblende, comparable to that described by Thomson *et al.* (1992), is fairly widespread in mafic gneiss.

The gneissic foliation in the host rocks probably formed at or near 'peak' thermal conditions (cf. Rodgers, 1981); it strikes northeast–southwest and dips between about 40° and 80° north-west. Strike faults and associated mylonite zones (e.g. Fig. 1) have not been observed where the veins are exposed (Fig. 2).

Physical properties of the vein system

The mafic gneiss is cut by a system of throughgoing, interconnected veins. A representative exposure is shown in Fig. 3. The total relief in the field area is about 30 m; the veins are exposed throughout this elevation interval. Most of the veins strike *c.* 170° and have subvertical dips, although rare, nearly horizontal ones that strike *c.* 90° and dip *c.* 15° north also occur. Consistent cross-cutting relations between these vein sets have not been recognized. The veins are not folded, and they clearly cross-cut the gneissic foliation of the host rocks. The distance between the walls of a given vein varies along its length; average vein widths are generally in the range 1 mm to 3 cm. The veins have well-defined terminations that resemble typical crack tips (cf. Lacazette & Engelder, 1992, and references therein). The most striking feature of the veins is that substantial open space is present between their walls *today* in outcrop (Figs 4 & 5). The open zones may be open continuously over vein surface areas as great

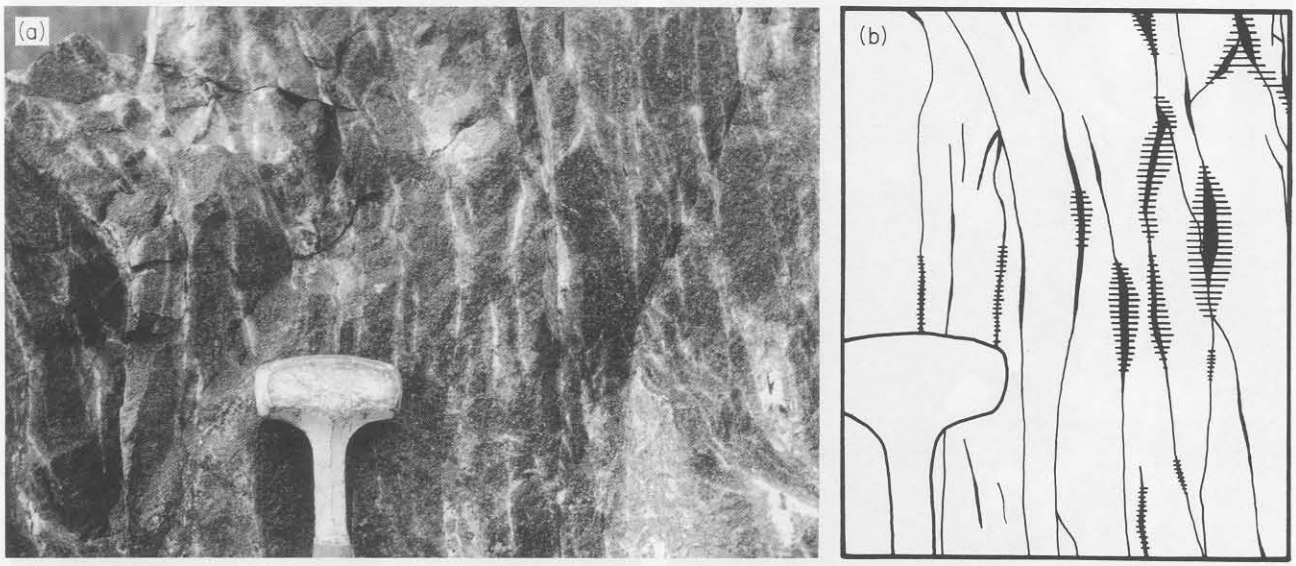

Fig. 3. (a) Typical field appearance of hydrothermal veins (vertical) cutting dark grey mafic gneiss wallrock. Veins comprise about 3 vol.% of the exposure. Light grey areas surrounding the veins are wallrock alteration zones (selvages). Hammer head is 10 cm wide. (b) Drawing of the central part of (a). Veins are black; largest, best-developed selvages are indicated by the horizontal rule. Note that selvages are widest adjacent to the widest parts of veins.

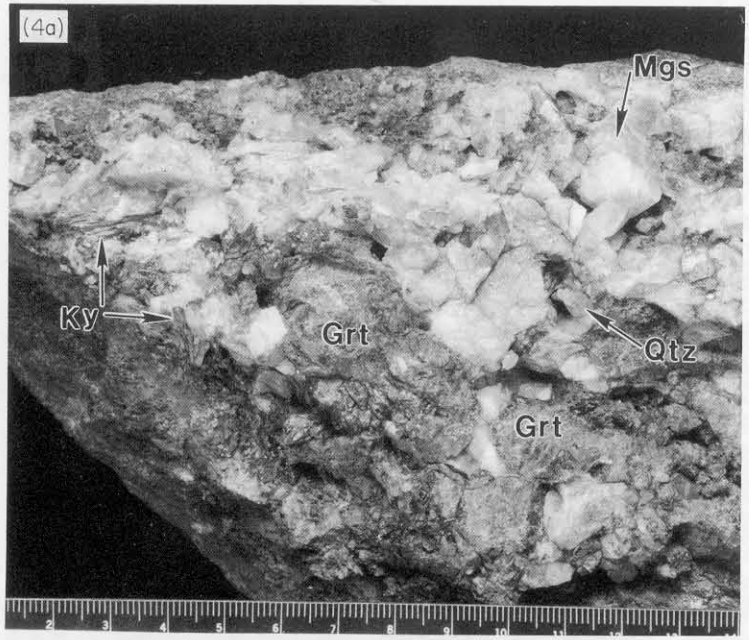

(4b)

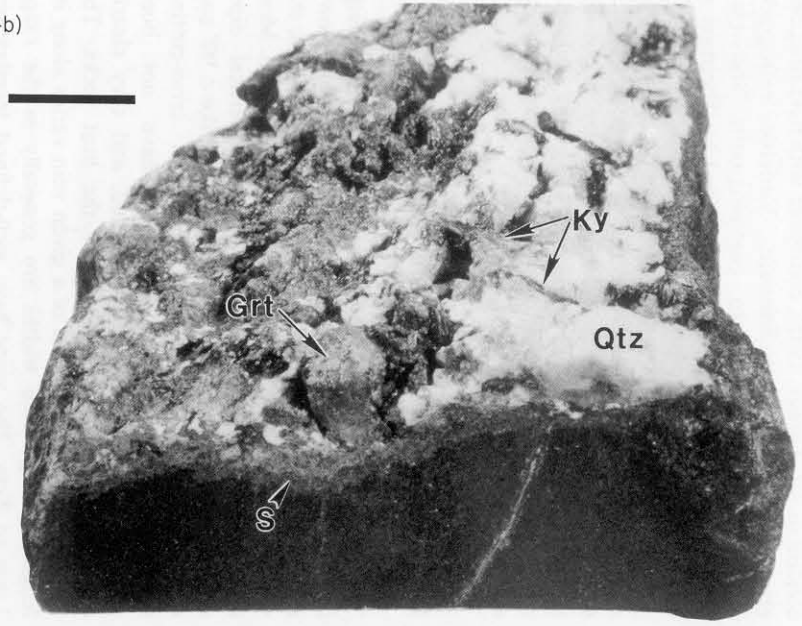

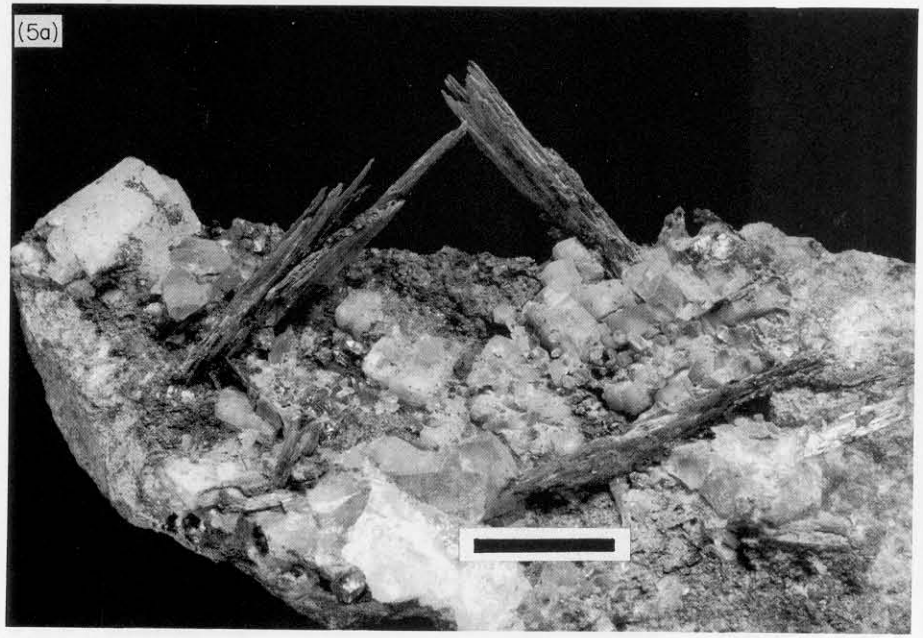

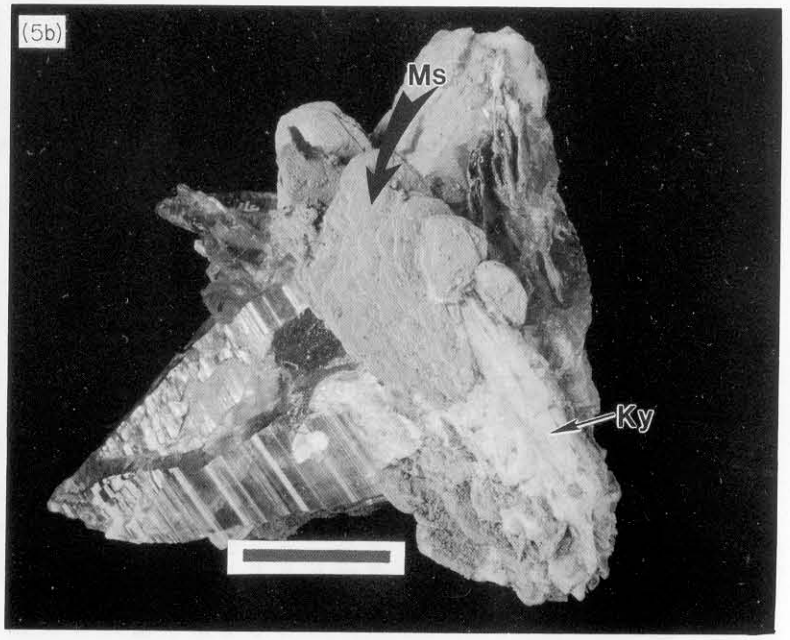

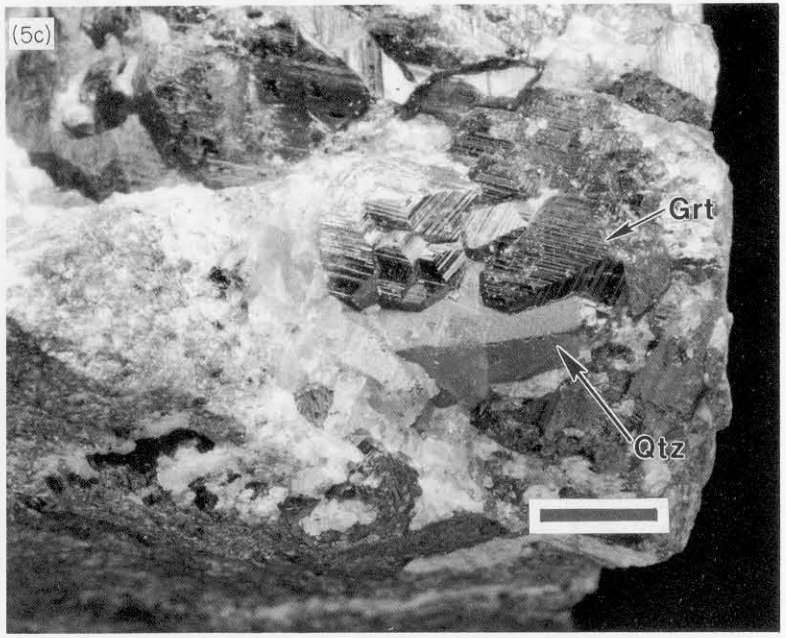

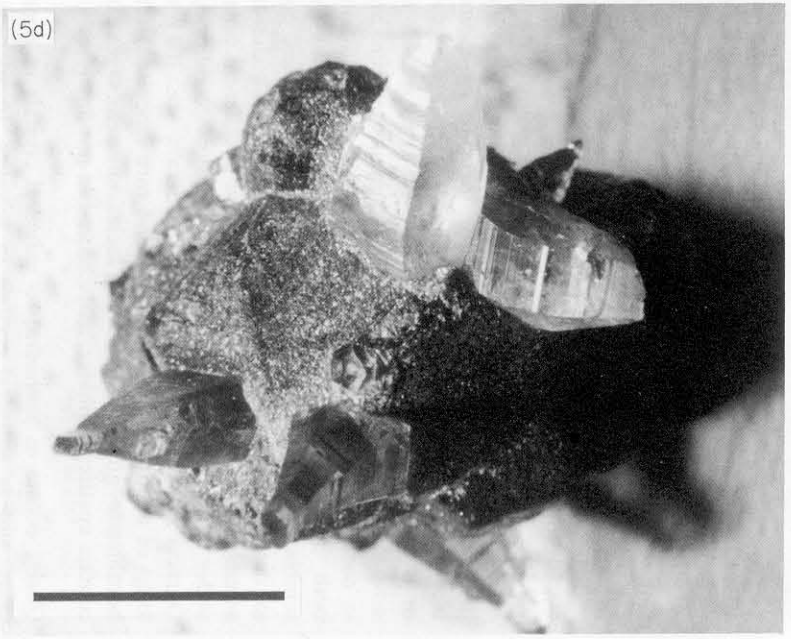

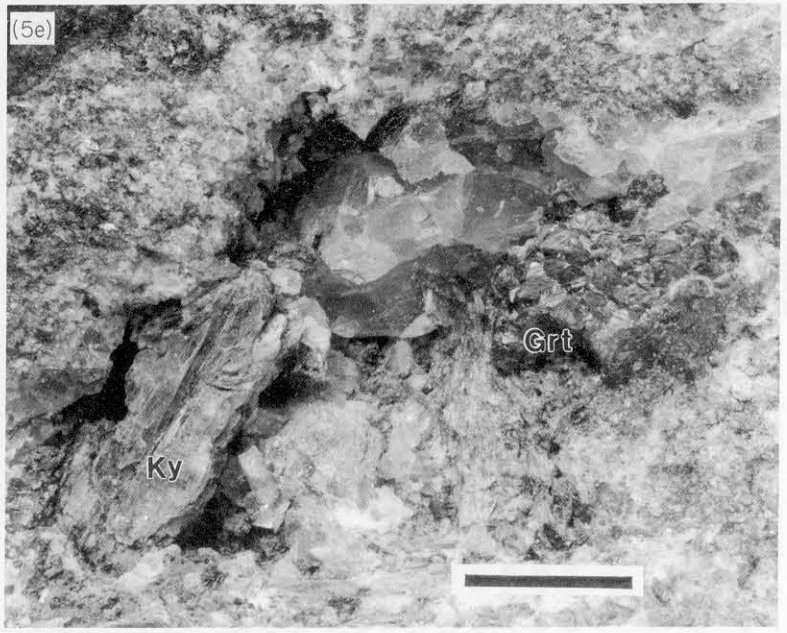

Fig. 4. Typical appearance of vein surfaces. (a) View perpendicular to a vein surface illustrating intergrowth of kyanite, garnet, quartz and magnesite. Some biotite and plagioclase are also present. Note substantial pore space between the individual crystals. Scale bar in centimetres. (b) Oblique view of the specimen shown in (a) looking towards a surface cut perpendicular to the vein–wallrock contact. Note the extreme mineralogical and textural differences between the vein minerals and the dark grey mafic gneiss (Pl + Cpx + Opx + Bt + Cum) wallrock. Alteration selvage adjacent to vein denoted by capital S. Small veinlet in central-right portion of specimen cross-cuts the main vein. Scale bar = 3 cm.

Fig. 5. Textures indicative of mineral growth into an environment of macroscopic open space between vein walls. (a) Euhedral kyanite blades, quartz crystals and magnesite rhombs which grew from a fracture surface. Scale bar = 1 cm. (b) Intergrowth of euhedral quartz (striated growth faces), kyanite (Ky) and muscovite (Ms). Muscovite has earthy lustre because its surface has been largely altered to fine-grained clay minerals. Note the tapering 'Tessin' habit of the quartz crystals. Scale bar = 1 cm. (c) Intimate intergrowth of euhedral quartz (Qtz) and garnet (Grt; striated growth faces) crystals projecting from a fracture surface. Scale bar = 0.5 cm. (d) Intimate intergrowth of euhedral quartz and garnet crystals. Specimen is resting on a wooden table top. Scale bar = 1 cm. (e) Coexisting kyanite (Ky) and garnet (Grt). View is perpendicular to fracture surface. Scale bar = 1 cm.

as *c.* 4 m^2. The veins are surrounded by a zone of altered wallrock (selvage) ranging from about 1 mm to several centimetres in width (Fig. 3). The selvages tend to be widest adjacent to the widest portions of the veins, and the most altered wallrocks are found where several veins form an anastomosing network (e.g. right portion of Fig. 3b).

Vein frequencies range from *c.* 1 to *c.* 20 m^{-1}. Veins (not including selvages) make up about 2% of the total rock mass (e.g. Fig. 3). The overall porosity of the rock mass (preserved as open space between vein walls *today*) is, on average, about 0.3%.

Minor late veinlets with subvertical dips are present in a few samples. The veinlets cross-cut the main set of veins at high angles, are narrow (<*c.* 2 mm wide), are composed mostly of magnesite and sulphides, and generally preserve no open space between their walls (Fig. 4b). In the following discussion, attention is focused on the major open veins described above; the veinlets will not be discussed further.

Vein and selvage mineral assemblages

The mineral assemblages in the veins and their adjacent selvages contrast strongly with those in the mafic wallrock gneiss (Fig. 4b). The veins are characterized by intimately intergrown, subhedral to euhedral crystals of quartz, garnet, biotite, kyanite and carbonate minerals which project out into open cavities along the vein walls (Figs 4–6). Typical mineral assemblages are

quartz + almandine-rich garnet
+ kyanite + magnesite + biotite + plagioclase (*c.* An_{20-40})
± ankerite ± muscovite (A)

and

quartz + almandine-rich garnet
+ hornblende + magnesite + plagioclase (*c.* An_{20-40})
± ankerite ± biotite. (B)

Assemblage (A) is considerably more common than assemblage (B). A few samples contain coexisting hornblende and kyanite, but these minerals generally do not occur together. Accessory minerals include staurolite, apatite, tourmaline, zircon, ilmenite, pyrrhotite and chalcopyrite. The mineral assemblages in the selvages are the same as those in the adjacent veins. Because the vein mineralogy is characteristic of the amphibolite facies of metamorphism, temperatures of formation were probably at least *c.* 500° C (cf. Turner 1981). The presence of kyanite in vein parageneses simultaneously constrains pressures to be in excess of *c.* 0.4 GPa.

Vein mineral compositions and key petrographic relations

Garnets range in size from *c.* 2 mm to *c.* 7 cm in diameter, and are compositionally zoned. As shown in Fig. 7, Ca/Fe and Mg/Fe decrease as garnet rims are approached. Garnet rims in contact with mineral assemblages in open veins have essentially the same composition as rims in contact with selvages (Fig. 7). High-contrast backscattered electron imaging reveals that garnet Ca/Fe and Mg/Fe also decrease in regions surrounding cross-cutting microcracks (Fig. 8). The above observations strongly suggest that garnet cores preserve original growth compositions, whereas the rims and areas around microcracks were chemically altered after growth had finished.

Many of the garnets that line open veins contain assemblages of mineral inclusions (e.g. Fig. 5c,d). The inclusion assemblages are generally the same as assemblages in contact with the garnet rims (e.g. assemblages A or B discussed above). However, the cores of garnets in several samples contain hornblende, whereas their rims are in contact with kyanite-bearing parageneses. In addition, both hornblende- and kyanite-bearing inclusion assemblages are present in sample JAQ-11, but they are not in contact with each other. The contrasting inclusion assemblages in JAQ-11 probably formed at different times under different chemical and/or physical conditions. Garnets may also have inclusions (generally <*c.* 100 μm long) of apatite, zircon, sulphides and rare ilmenite. Both hornblende- and kyanite-bearing inclusion assemblages can contain apatite, sulphides, and zircon, but not ilmenite.

Quartz occurs as subhedral to euhedral crystals in open veins, and as anhedral crystals in selvages. In addition, most garnets in open veins contain subhedral to euhedral quartz inclusions. Crystals range in length from *c.* 1 mm or less in selvages, to several centimetres in open veins. Euhedral crystals generally have the tapering wedge-form of the 'Tessin' habit (Fig. 5b,d; cf. Weibel, 1966). Textures indicative of intracrystalline deformation, such as undulose extinction and deformation bands, are absent.

Kyanite occurs as subhedral bladed crystals that are flattened parallel to (100) (Fig. 5a,b,e). Kyanite crystals in selvages or included within garnets range in length from *c.* 0.5 mm to *c.* 1 cm, whereas those in open veins may be as much as *c.* 5 cm long. Crystals in open veins have irregular, finger-like terminations (Fig. 5a). Reconnaissance microprobe analyses indicate that kyanite is nearly pure Al_2SiO_5 ($Fe_2O_3 + MnO + TiO_2 + V_2O_5 + Cr_2O_3 < c.$ 0.5 wt%).

Plagioclase is present as millimetre-scale, subhedral to anhedral crystals regardless of position in the vein–selvage system. Plagioclase grains may contain irregularly shaped domains of variable composition; the total variability in a given grain is typically less than $\pm An_4$. Plagioclase grains included within garnets are more albite-rich (An_{25-29}; average $\ln(Ca/Na) = -1.00 \pm 0.086$, 2σ) than those in selvages or open veins (An_{33-42}; average $\ln(Ca/Na) = -0.52 \pm 0.104$) (Table 3). The two averages are different at the 99.98% confidence level. See Aitchison (1989), Woronow & Love (1990) and Ague (1994a) for detailed discussions of the statistical analysis of compositional data. Plagioclase grains in the mafic gneiss (*c.* An_{70-80}) are much more calcic than those in open veins or selvages (cf. Table 3).

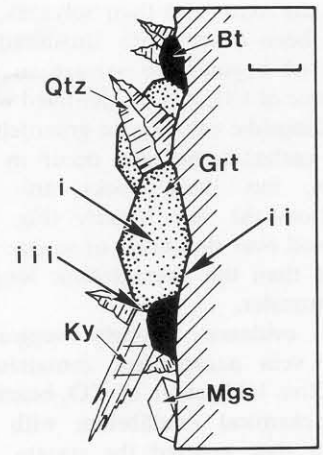

Fig. 6. Schematic drawing of some of the major fracture zone minerals and the assemblages used for thermobarometry. View is parallel to fracture surface. Zone of altered wallrock (selvage) is indicated by diagonal rule. The thermobarometry assemblages are: i, included within garnets; ii, in contact with garnet rims in selvages; iii, in contact with garnet rims in open fractures. For clarity, assemblage types i and ii are not drawn in detail. Scale bar = *c.* 1 cm.

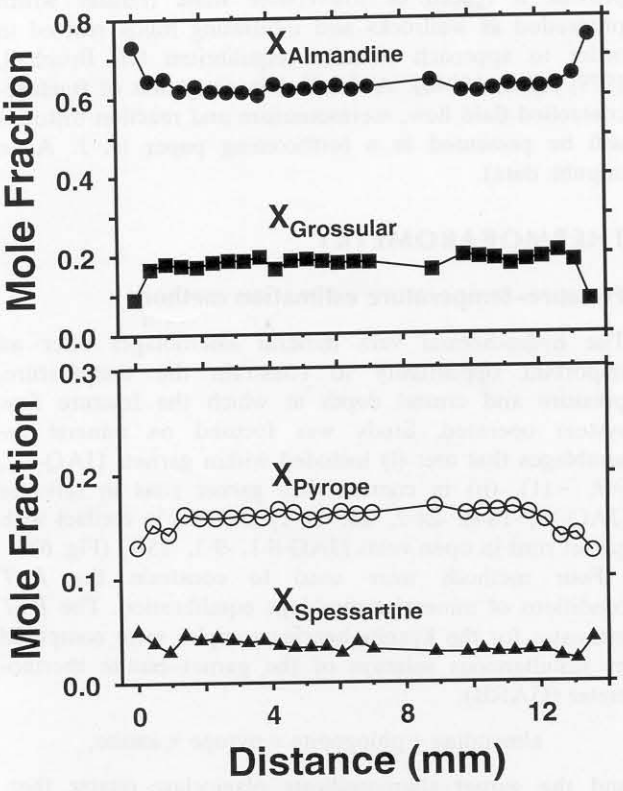

Fig. 7. Compositional profiles across hydrothermal garnet in sample JAQ-24-2. Left and right sides of the profiles are in contact with selvage kyanite and open fracture, respectively. Note pronounced decreases in Mg/Fe and Ca/Fe at the garnet rims. Data points are sparse in the region between $x = 7$ and 10 mm because it is largely occupied by inclusions of euhedral quartz.

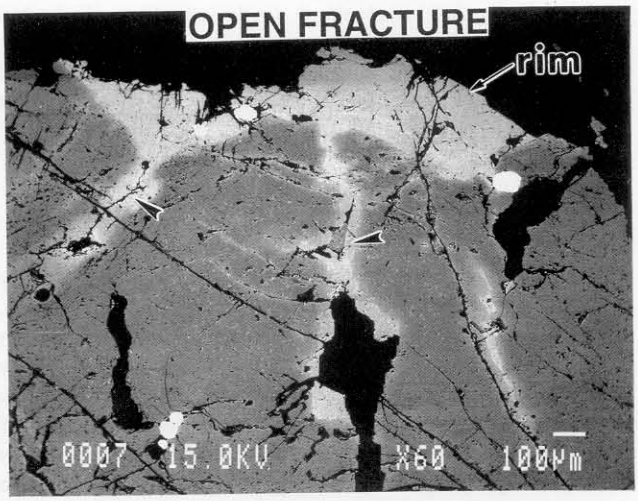

Fig. 8. Backscattered electron image of chemical variations in a fracture zone garnet (sample JAQ-24-2). Open fracture appears black and runs across the top of the photograph. The garnet rim and areas around microcracks which extend inwards from the rim (e.g. arrowheads) appear light grey because they have significantly lower Mg/Fe and Ca/Fe than the rest of the garnet. Rims and regions around microcracks are interpreted to have been chemically altered after the garnets grew (see text). The three large black regions within the garnet are inclusions of plagioclase ± quartz. Small white inclusions are zircons. Garnet rim does not appear perfectly euhedral because it was damaged slightly during sample preparation.

Hornblende occurs as subhedral to euhedral crystals *c.* 0.1 mm to *c.* 1 cm long. Chemical zonation has not been observed.

Biotite and *muscovite* generally range from a few tenths of a millimetre to about 1 cm in length, and are unzoned. The Ti content of biotite in the veins and selvages (*c.* 1.2–2.0 wt%) is significantly lower than that of biotite in the mafic gneiss wallrock (*c.* 3–4 wt%). Muscovite coexists only with kyanite-bearing assemblages. Muscovite inclusions within garnets contain less Mg, Fe and Ti, and more Al and Na than do grains in open veins or selvages (Table 5).

Carbonate minerals are found as subhedral to euhedral rhombs in open veins and within garnets, and as subhedral to anhedral crystals in selvages. Grain size ranges from several hundred micrometres to several centimetres. The most common carbonate is magnesite. Reconnaissance microprobe analyses indicate that magnesite compositions vary between about $Mg_{0.70-0.95}Fe_{0.30-0.05}CO_3$. However, in a few samples, the outermost rims of magnesite crystals in open veins grade to compositions that are nearly pure siderite. Ankerite and magnesite occur together in some samples.

Fluid inclusions are widespread in garnet, quartz and carbonate minerals. They occur principally on euhedral growth facies, but they are also abundant along cross-cutting microcracks which appear to have formed after the minerals grew.

Retrograde alteration of vein biotite, garnet and kyanite to assemblages containing various combinations of sericite,

chlorite and clay minerals is fairly common. Euhedral crystals of calcite and/or pyrite are found coating assemblages (A) and (B) in some veins. The calcite and pyrite growth is interpreted to be a late phenomenon that post-dates the amphibolite facies vein assemblages.

VEIN MINERAL GROWTH INTO MACROSCOPIC OPEN SPACE

Quartz is the key mineral whose textural relations clarify the environment of vein mineral assemblage growth. Quartz is a low-density framework silicate which, in general, develops as well-formed euhedral prisms only when it grows unrestricted into fluid-filled space (Williams *et al.*, 1982, pp. 438–439). The small euhedral crystals of authigenic quartz which replace calcite in some limestones are the only exception to this general rule. The intimate intergrowth of euhedral quartz, kyanite and garnet crystals establishes that each of the minerals must have grown into an environment of *macroscopic open space* between the vein walls (Figs 4 & 5). Fluid or mineral inclusion trails consistent with the 'crack-seal' mechanism of vein formation are absent from the 43 thin sections examined, as are fibrous syntaxial or antitaxial mineral growth habits (cf. Durney & Ramsay, 1973; Ramsay, 1980). Therefore, the veins did not form by repeated episodes of opening at the micrometre-scale followed by 'healing' caused by mineral precipitation.

The occurrence of kyanite in the vein mineral assemblages and the conclusion that it grew into fluid-filled open space deserves further comment. Kyanite is relatively common in the quartz veins of metamorphic rocks (cf. Kerrick, 1990, Chapter 10, and references therein). Kyanite generally occurs as sub- to euhedral bladed crystals in veins, but this habit is not diagnostic of original open space growth conditions because kyanite will always tend to develop idioblastic surfaces at contacts with quartz (Williams *et al.*, 1982, pp. 438–439).

Quartz + kyanite veins commonly have widths in the centimetre to metre range, but these widths need not directly reflect fracture apertures at the time of fluid flow. Veins record the time-integrated history of flow and mass transfer, and large vein structures can be built up by repeated microfracturing and precipitation according to the crack-seal mechanism (Ramsay, 1980; Walther, 1990). Unequivocal examples of quartz and kyanite growth into macroscopic open space between vein walls are rare, but several have been documented (cf. Miyashiro, 1951; Kerrick, 1990, pp. 325–326). However, these previously recognized examples are not necessarily indicative of deep crustal mass transfer because quartz + kyanite is stable at pressures and corresponding depths as low as *c.* 0.23 GPa and *c.* 8 km, respectively (calculations done using the thermodynamic data of Berman, 1988).

IMPLICATIONS FOR MASS TRANSPORT

The vein mineral assemblages place constraints on fluid behaviour in the system. Although carbonate minerals are widespread in the veins and their selvages, no carbonate minerals have been observed in 'unaltered' mafic gneiss wallrocks located beyond the selvage margins, and no other local source of CO_2 can be identified where the veins are exposed. Diopsidic calc-silicate granofels layers, some of which are carbonate-bearing, occur in some of the adjacent units, but these rocks are far removed (0.5–1.0 km) from the vein locality (Fig. 2). The vein system is exposed over thousands of square metres, which is much larger than the characteristic length scales for diffusive mass transfer.

The above evidence strongly suggests that the production of vein parageneses containing carbonates required advective infiltration of CO_2-bearing fluids that were out of chemical equilibrium with mafic gneiss wallrocks when they entered the system. The simplest interpretation of the field relations is that the veins were originally fractures through which the fluids flowed. Because the vein minerals grew into open space along the vein walls and are not deformed, present-day vein widths almost certainly represent original fracture apertures. The most intense mineralization and wallrock alteration is found where the veins are widest (Fig. 3), which suggests that fluid flow was preferentially channellized along the widest (and therefore most permeable) portions of the fractures. The vein and selvage mineral assemblages provide a record of irreversible mass transfer which proceeded as wallrocks and infiltrating fluids reacted in order to approach chemical equilibrium (cf. Brimhall, 1979; Ague, 1994b). A detailed investigation of fracture-controlled fluid flow, metasomatism and reaction histories will be presented in a forthcoming paper (J. J. Ague unpubl. data).

THERMOBAROMETRY

Pressure–temperature estimation methods

The hydrothermal vein mineral assemblages offer an important opportunity to constrain the temperature, pressure and crustal depth at which the fracture flow system operated. Study was focused on mineral assemblages that are: (i) included within garnets (JAQ-3-2, −7, −11), (ii) in contact with garnet rims in selvages (JAQ-10, -18-sl, -24-2, -25, -26-1) and (iii) in contact with garnet rims in open veins (JAQ-8-1, -9-1, -15-1) (Fig. 6).

Four methods were used to constrain the *P–T* conditions of mineral assemblage equilibration. The *P–T* estimates for the kyanite-bearing samples were computed by simultaneous solution of the garnet–biotite thermometer (GARB):

$$\text{almandine} + \text{phlogopite} = \text{pyrope} + \text{annite},$$

and the garnet–aluminosilicate–plagioclase–quartz thermobarometer (GASP):

$$3\text{anorthite} = \text{grossular} + 2\text{kyanite} + \text{quartz}$$

(Method I). Method I employs the calibrations of Ferry & Spear (1978) and Koziol & Newton (1988) for GARB and

GASP, respectively, in conjunction with an ideal solution model for biotite and the activity models of Hodges & Royden (1984) for garnet and Newton & Haselton (1981) for plagioclase. Samples JAQ-7 and -25 contain muscovite in textural equilibrium with the GARB and GASP assemblages. This facilitates application of the SGAM thermobarometer, which involves GARB and the following two equilibria (McMullin *et al.*, 1991):

almandine + muscovite = annite + 2kyanite + quartz

and

phlogopite + 2kyanite + quartz = pyrope + muscovite.

Method II P–T estimates were obtained by simultaneous solution of the GARB, GASP and SGAM equilibria using the TWEEQU software package of Berman (1991). TWEEQU incorporates the internally consistent thermodynamic data of Berman (1988, 1990), Mäder & Berman (1991) and McMullin *et al.* (1991). Activity–composition relations for garnet, muscovite–paragonite, biotite and plagioclase were computed using the models of Berman (1990), Chatterjee & Froese (1975), McMullin *et al.* (1991) and Furhman & Lindsley (1988), respectively. The biotite activity model of McMullin *et al.* (1991) was modified slightly by assuming that $X_K^{Bt} = K/1.0$ (structural formula on an 11 oxygen basis; R. G. Berman, pers. comm., 1992). Equilibration P–T conditions were estimated for hornblende-bearing assemblages using the garnet–hornblende–plagioclase–quartz barometer calibrations and recommended activity models of Kohn & Spear (1990) in conjunction with GARB (Method III) or, if biotite was absent from the assemblage, the garnet–hornblende thermometer of Graham & Powell (1984) (Method IV). Method III and IV pressure estimates are averages of results from the Fe- and Mg-end-member barometers of Kohn & Spear (1990). Method IV temperature estimates probably have greater overall uncertainties than those of the other methods owing to the simple activity–composition relations for garnet and hornblende used by Graham & Powell (1984). Quartz and kyanite activities were set to one in the calculations.

The precision of the P–T estimates must be known so that results from different samples may be compared. Uncertainties due to random errors of analysis and real variations in mineral compositions were propagated through the thermobarometric equations of Methods I, III and IV using bootstrap statistical techniques (Efron, 1982; Ague & Brandon, 1992; Ague, 1994a). Average mole fractions used in the bootstrap analysis were computed with the measure of location advocated by Aitchison (1989), in order to account for the closure problem and the multivariate nature of compositional data. The calculated uncertainties reflect the precision of mean P–T estimates, not the inaccuracies associated with activity models or end-member reaction calibrations (e.g. Hodges & McKenna, 1987). Although calculated precision limits will change somewhat depending upon the activity models used, interpretation of P–T histories should not be significantly affected. For example, discrepancies between GARB–GASP P–T estimates calculated using Method I and TWEEQU are $<$*c.* 0.03 GPa and *c.* 20° C, regardless of mineral composition.

For Method II, a measure of uncertainty is provided by the ranges in P–T over which the calculated GARB, GASP and SGAM equilibrium curves intersect (Berman, 1991).

Results

Mineral assemblages included within garnets and mineral assemblages in contact with garnet rims define two P–T fields that are distinct from each other (Figs 9 & 10). Average P–T conditions for the inclusion assemblages are *c.* 560° C and *c.* 0.8 GPa, whereas the averages for the rim assemblages are *c.* 500° C and *c.* 0.4 GPa (Table 6). The differences in average P–T are large enough to be accurately resolved by comparative thermobarometry (cf. Hodges & McKenna, 1987; Berman, 1991), and cannot be explained by analytical uncertainty alone (Fig. 9).

Independent P–T estimates for samples suitable for application of multiple thermometers or barometers agree well with each other. For example, because both kyanite- and hornblende-bearing assemblages are included within garnets in JAQ-11, Methods I and III can be used. Results for the two methods differ by only 31 °C and 0.08 GPa (Table 6; Fig. 9). Assemblages in samples JAQ-7 and -25 are suitable for Method II. For both samples, the calculated GARB, GASP and SGAM equilibria intersect over a very small region of P–T space (Fig. 10). The

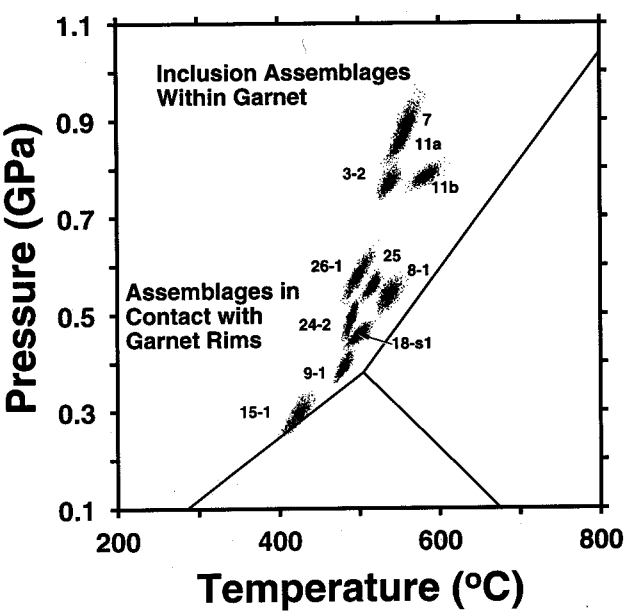

Fig. 9. Results of bootstrap P–T calculations for methods I, III and IV. Mean P–T estimates are indicated by the black dots, and the elliptical clouds of 'bootstrap replicates' which surround them closely approximate 95% confidence regions (cf. Efron, 1982; Ague & Brandon, 1992; Ague, 1994a). Note that inclusion assemblages within garnets preserve a significantly higher P–T signature than assemblages in contact with garnet rims.

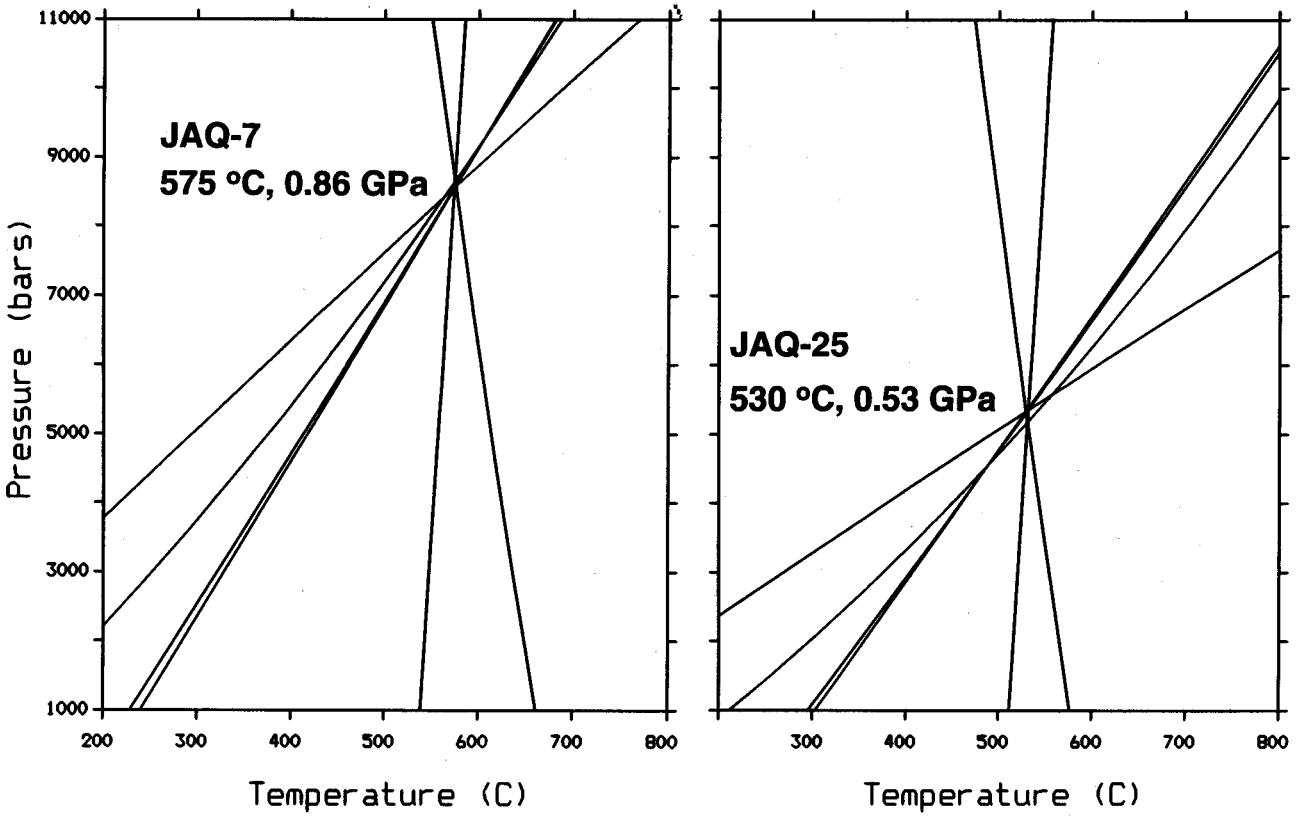

Fig. 10. Method II (GARB–GASP–SGAM) results for samples JAQ-7 and -25 computed using the TWEEQU software of Berman (1991). The graphs include all equilibria, both stable and metastable, that can be calculated for the assemblage Bt + Ms + Ky + Grt + Qtz + Pl (see McMullin *et al.*, 1991, for detailed discussion). Equilibria are unlabelled for clarity. The analysed assemblages in JAQ-7 and -25 probably represent a close approach to equilibrium, because their respective equilibrium curves intersect over very small regions of *P–T* space. Note that the assemblage included within garnets in JAQ-7 preserves a much higher pressure of equilibration than does the assemblage in contact with garnet rims in JAQ-25.

internal consistency of *P–T* estimates obtained from independent thermometers and barometers strongly suggests that measured mineral compositions record conditions when local fluid–rock equilibrium was attained or closely approached.

DISCUSSION

Interpretation of *P–T* estimates

Backscattered electron images and compositional analysis of garnet (Figs 7 & 8) indicate that garnet interiors

Table 6. *T* (°C) and *P* (GPa) estimates.

Sample	Type*	Assemb-lage†	Method I		Method II		Method III		Method IV	
			T	*P*	*T*	*P*	*T*	*P*	*T*	*P*
JAQ-3-2	i	C	—	—	—	—	—	—	538	0.77
JAQ-7	i	A,B	559	0.89	575	0.86	—	—	—	—
JAQ-8-1	iii	A	537	0.54	—	—	—	—	—	—
JAQ-9-1	iii	A	481	0.39	—	—	—	—	—	—
JAQ-11a	i	A	553	0.86	—	—	—	—	—	—
JAQ-11b	i	D	—	—	—	—	584	0.78	—	—
JAQ-15-1	iii	A	424	0.30	—	—	—	—	—	—
JAQ-18-sl	ii	A	499	0.46	—	—	—	—	—	—
JAQ-24-2	ii	A	490	0.49	—	—	—	—	—	—
JAQ-25	ii	A,B	517	0.56	530	0.53	—	—	—	—
JAQ-26-1	ii	C	—	—	—	—	—	—	499	0.58

* Assemblage type. i, inclusions within garnet; ii, in contact with garnet rim in selvage; iii, in contact with garnet rim in open vein.

† Mineral assemblage used for thermobarometry. A, Grt + Ky + Qtz + Bt + Pl; B, Grt + Ky + Qtz + Bt + Pl + Ms; C, Grt + Qtz + Pl + Hbl; D, Grt + Qtz + Pl + Hbl + Bt.

preserve original growth compositions, whereas rims and areas around microcracks were altered after growth had finished. Therefore, inclusion assemblages within garnets probably provide the best estimate of P–T conditions attending fracture formation (*c.* 560° C and *c.* 0.8 GPa).

Of critical importance is determining if the high equilibration pressures are a consequence of mineral growth in the deep crust or of fluid overpressures at shallower crustal levels. Results from fluid inclusion studies (cf. Sisson & Hollister, 1990) suggest that fluid pressure can exceed lithostatic pressure by 0.1 GPa or more during orogenesis. The high fluid pressures may result from fluid production by devolatization reactions (e.g. Yardley, 1986) and/or tectonism (e.g. Vrolijk, 1987; Nur & Walder, 1990). As deformation and metamorphism proceed, the rocks eventually fail, the overpressured fluid escapes and residual fluid pressure in the system falls to levels at or below lithostatic pressure. Continued deformation and metamorphism causes the cycle of fluid pressure buildup and release to be repeated many times (e.g. Yardley, 1986; Nur & Walder, 1990). Metamorphic minerals that grow in environments where fluid pressures cycle over a large range (±0.1 GPa or more) should have oscillatory compositional growth zonation. For the veins studied here, the zonation would be preserved in garnet and hornblende, because temperatures of vein formation were far below those required to cause complete compositional homogenization by intracrystalline diffusion (cf. Cygan & Lasaga, 1985; Hammarstrom & Zen, 1986). However, oscillatory zonation has not been observed in any of the vein minerals (cf. Fig. 7). I conclude that although increases in fluid pressure above lithostatic pressure may have been part of the fluid flow process, they were not large enough to account for the high pressures of vein mineral assemblage equilibration. Therefore, the thermobarometry results for mineral inclusion assemblages within garnets are interpreted to reflect fracturing, fluid flow and vein growth at deep crustal levels of *c.* 30 km.

Because the fractures were open at depths in excess of 15 km, they were almost certainly held open by a fluid phase (cf. Walther, 1990). Mineral assemblages in contact with garnet rims in selvages and open veins would have been exposed to fracture fluids for longer times than assemblages included within garents. In a fluid-rich environment, intercrystalline diffusion is enhanced, and extensive re-equilibration of mineral compositions in response to changing P–T–X conditions can occur. Therefore, minerals in contact with garnet rims are interpreted to have equilibrated with each other during exhumation-related cooling and decompression after the fractures were formed. Because garnet rims have lower grossular content than garnet interiors, and plagioclase in contact with garnet rims has higher anorthite content than plagioclase inclusions within garnet, equilibration may have involved coupled Ca exchange between garnet and plagioclase via reactions such as GASP. However, Ca and other elements may also have been transported into or out of the system by fracture-controlled fluid flow during exhumation. The variable retrograde alteration of vein biotite, garnet and kyanite to sericite, chlorite and clay minerals suggests that fluids were present in some of the fractures to very low temperatures and crustal depths.

It is extremely unlikely that the fractures were conduits for silicate melts, because the maximum temperature estimates for vein assemblages are about 100° C less than the water-saturated tonalite solidus. Furthermore, cooling of known silicate or carbonatite magma types will not produce the observed vein mineral assemblages.

Comparison with the P–T path and tectonic history of the Merrimack synclinorium

Previous workers, including Schumacher *et al.* (1989), Armstrong *et al.* (1992) and Thomson *et al.* (1992), among others, have concluded that the Merrimack synclinorium was metamorphosed along an anticlockwise P–T path which started in the andalusite stability field and reached peak thermal conditions in the granulite facies (Fig. 11). The petrological relations of the fracture zone host rocks (e.g. sillimanite pseudomorphs after andalusite; granulite facies metamorphism) are consistent with this P–T history. Following granulite facies metamorphism, burial and compression of the synclinorium continued while it cooled to amphibolite facies temperatures within the stability field of kyanite (Fig. 11; Schumacher *et al.*, 1989; Armstrong *et*

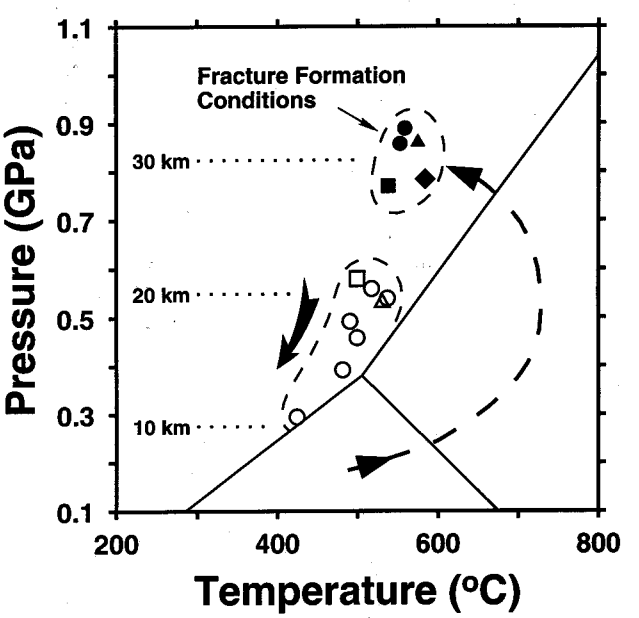

Fig. 11. P–T estimates compared with the previously determined P–T path of the Merrimack synclinorium. Anticlockwise P–T path discussed by Schumacher *et al.* (1989), Armstrong *et al.* (1992) and Thomson *et al.* (1992) shown with heavy dashed line. Inferred conditions of fracture formation correspond to the greatest depth of burial of the synclinorium. Possible exhumation path is indicated by the large black arrow (cf. Armstrong *et al.*, 1992). Filled symbols, assemblages included within garnets; open symbols, assemblages in contact with garnet rims. Circles, Method I; triangles, Method II; diamonds, Method III; squares, Method IV. Depth of burial computed using an average crustal density of 2800 kg m^{-3}. See text for further discussion.

al., 1992). The estimated conditions of fracture formation (*c.* 560° C, *c.* 0.8 GPa) lie along this part of the *P–T* path, and correspond to the maximum pressure and crustal depth reached by the synclinorium (*c.* 30 km).

The tectonic regime leading to fracturing and vein growth remains to be determined, but some potentially important relations can be highlighted. The timing of fracturing deduced from the *P–T* path (Fig. 11) is consistent with the observation that the fractures cross-cut (and therefore post-date) the gneissic fabric of their granulite facies host rocks. The *P–T* conditions of fracturing correspond to those attending regional mylonite formation along the major NE–SW-trending faults that cut the synclinorium (Fig. 1). Furthermore, the roughly N–S strike of the main set of veins is subparallel to that of numerous small, subvertical cross-faults that run between the major faults (Peper & Pease, 1975; Fig. 2). Peper & Pease (1975) inferred that most of these smaller faults are normal faults, and reported that large flakes of retrograde muscovite are commonly found on the fault surfaces. The exact sequence of faulting is not known, but Peper & Pease (1975) noted that some of the cross-faults terminate against the major NE–SW-trending faults. The above relations indicate that the veins could have developed during the formation of the major NE–SW-trending faults, or sometime thereafter. The large retrograde muscovite crystals associated with the smaller, dominantly N–S-trending cross-faults demonstrate that fluid infiltration occurred along faults in the region. Because the main vein set and many of the cross-faults have similar orientations, they may be genetically related. One, admittedly speculative, scenario consistent with available evidence is that veining and the required increases in volume were associated with the initial phases of exhumation of the synclinorium.

The *P–T* estimates from mineral assemblages in contact with garnet rims place new constraints on the exhumation path of the synclinorium. Thermobarometry suggests that the area was at temperatures of *c.* 500° C as it was exhumed through the 20–15 km depth interval (Fig. 11). This result is comparable with the exhumation path postulated for the synclinorium by Armstrong *et al.* (1992). Whether fluid flow occurred throughout exhumation or was restricted to the deep crustal levels where the fractures formed is presently unknown.

Implications for deep crustal permeability and porosity

The extreme chemical alteration that took place along the fracture walls and adjacent selvages (e.g. Fig. 4) provides strong evidence that the fractures were major fluid conduits having permeabilities well in excess of the mafic gneiss host rocks (cf. Ferry & Dipple, 1991). Rock failure producing large-aperture fractures could have dramatic transient effects on the permeability of the lower crust (cf. Sibson *et al.*, 1988). A rough order of magnitude estimate of the intrinsic fracture permeability, k_f, of a rock mass can be obtained using the expression: $k_f = (nd^3)/12$, where n and d are the average frequencies and apertures of the fractures, respectively (Norton & Knapp, 1977). Taking d to be 1 mm, a representative value for the system described here, k_f estimates range from *c.* 10^{-13} to *c.* 10^{-10} m^2 for values of n between 1 and 1000 km^{-1}. The k_f estimates are a factor of 10^3–10^{12} larger than the permeabilities that are generally assumed for deeply seated rocks (cf. England & Thompson, 1984).

Determining the porosity of the system when it was active requires detailed knowledge of the timing of fracture opening. Although the sequence of fracturing events remains to be established, some constraints can be placed on the porosity of the original system. The total volume of veins provides an upper limit for the original fracture porosity if it is assumed that all the fractures were open simultaneously; field measurements indicate that veins comprise about 2% of the rock mass (e.g. Fig. 3). The porosity preserved as open space between fracture *today* (*c.* 0.3%) reflects the final state of the system in the deep crust. This amount of porosity may be smaller than that which attended fluid flow because the fractures are now partially or completely filled with minerals.

CONCLUDING REMARKS

The results of this study indicate that large-aperture, fluid-filled fractures can be present in continental orogens to depths of *c.* 30 km. Furthermore, because the fractures are zones of elevated permeability, they can facilitate fluid flow and metasomatic alteration of wallrocks (cf. Ague, 1991, 1994a,b).

Evidence from geophysical studies strongly suggests that fracturing is common at middle to lower crustal levels in continental orogenic belts. For example, from April 1980 through February 1994, 1076 seismic events were recorded at depths of 20–35 km in the Los Angeles area (data from the California Institute of Technology Earthquake Catalog). In addition, seismic events routinely occur over the 20–35 km depth range in continental crust along the convergent margin in western Washington State (cf. Lees & Crowder, 1990). Moreover, results from a variety of seismic and magnetotelluric investigations suggest that fluid-filled fractures and pores comprising as much as several percent porosity may be widespread in middle to lower continental crust (cf. Matthews & Cheadle, 1986; Hyndman & Shearer, 1989). Consequently, it is tempting to speculate that networks of large-aperture fractures play a significant role in deep crustal hydrological systems, and that their importance has been greatly underestimated.

ACKNOWLEDGEMENTS

I thank M. T. Brandon, A. C. Lasaga, J. J. Park, D. M. Rye, B. J. Skinner and P. R. Bartholomew for many thoughtful discussions, N. M. S. Oliver and R. P. Wintsch for thorough and critical reviews, P. Brown, E. J. Essene, P. Philippot, J. Selverstone and V. B. Sisson for their insightful comments on earlier versions of the manuscript,

J. M. Lees for help with the California Institute of Technology Earthquake Catalog, B. Sacco for extraordinary photographic work, and W. C. Phelps for careful preparation of thin sections. R. J. Faux brought the field area to my attention. M. Harakaly, T. M. Harakaly and L. Becker kindly allowed access to the field area, and have provided generous logistic support. Financial support from Yale University and NSF grants EAR-8905016 and EAR-9118006 is gratefully acknowledged.

REFERENCES

Ague, J. J., 1991. Evidence for major mass transfer and volume strain during regional metamorphism of pelites. *Geology*, **19**, 855–858.

Ague, J. J., 1994a. Mass transfer during Barrovian metamorphism of pelites, south-central Connecticut. I. Evidence for changes in composition and volume. *American Journal of Science*, **294**, 989–1057.

Ague, J. J., 1994b. Mass transfer during Barrovian metamorphism of pelites, south-central Connecticut, II. Channelized fluid flow and the growth of staurolite and kyanite. *American Journal of Science*, **294**, 1061–1134.

Ague, J. J. & Brandon, M. T., 1992. Tilt and northward offset of Cordilleran batholiths resolved using igneous barometry. *Nature*, **360**, 146–149.

Aitchison, J., 1989. Measures of location of compositional data sets. *Mathematical Geology*, **21**, 787–790.

Armstrong, T. R., Tracy, R. J. & Hames, W. E., 1992. Contrasting styles of Taconian, eastern Acadian, and western Acadian metamorphism, central and western New England. *Journal of Metamorphic Geology*, **10**, 415–426.

Berman, R. G., 1988. Internally-consistent thermodynamic data for minerals in the system Na_2O–K_2O–CaO–MgO–FeO–Fe_2O_3–Al_2O_3–SiO_2–TiO_2–H_2O–CO_2. *Journal of Petrology*, **29**, 445–522.

Berman, R. G., 1990. Mixing properties of Ca–Mg–Fe–Mn garnets. *American Mineralogist*, **75**, 328–344.

Berman, R. G., 1991. Thermobarometry using multi-equilibrium calculations: a new technique, with petrological applications. *Canadian Mineralogist*, **29**, 833–855.

Berry, H. N., IV, 1992. Stratigraphy and structural geology in the Acadian granulite facies. In: *Guidebook for Fieldtrips in the Connecticut Valley Region of Massachusetts and Adjacent States* (eds Robinson, P. & Brady, J. B.), pp. 95–119. University of Massachusetts, Department of Geology and Geography, Contribution 66.

Brimhall, G. H., 1979. Lithologic determination of mass transfer mechanisms of multiple-stage porphyry copper mineralization at Butte, Montana; vein formation by hypogene leaching and enrichment of potassium silicate protore. *Economic Geology*, **74**, 556–589.

Chamberlain, C. P. & Rumble, D., 1988. Thermal anomalies in a regional metamorphic terrane: an isotopic study of the role of fluids. *Journal of Petrology*, **29**, 1215–1232.

Chatterjee, N. D. & Froese, E., 1975. A thermodynamic study of the pseudobinary join muscovite–paragonite in the system $KAlSi_3O_8$–$NaAlSi_3O_8$–Al_2O_3–SiO_2–H_2O. *American Mineralogist*, **60**, 985–993.

Cygan, R. T. & Lasaga, A. C., 1985. Self-diffusion of magnesium in garnet at 750° and 900° C. *American Journal of Science*, **285**, 328–350.

Durney, D. W. & Ramsay, J. G., 1973. Incremental strains measured by syntectonic crystal growths. In: *Gravity and Tectonics* (eds DeJong, K. E. & Scholten, R.), pp. 67–96. John Wiley and Sons, New York.

Efron, B., 1982. *The Jackknife, the Bootstrap, and other Resampling Plans*. Society for Industrial and Applied Mathematics, Philadelphia.

England, P. C. & Thompson, A. B., 1984. Pressure–temperature–time paths of regional metamorphism. I. Heat transfer during the evolution of regions of thickened continental crust. *Journal of Petrology*, **25**, 894–928.

Essene, E. J. & Fyfe, W. S., 1967. Omphacite in Californian metamorphic rocks. *Contributions to Mineralogy and Petrology*, **15**, 1–23.

Fahey, R. J. & Pease, M. H., 1977. Preliminary Bedrock Geologic Map of the South Coventry Quadrangle, Tolland County, Connecticut. *U.S. Geological Survey Open-File Report*, **77-584**.

Ferry, J. M. & Dipple, G. M., 1991. Fluid flow, mineral reactions, and metasomatism. *Geology*, **19**, 211–214.

Ferry, J. M. & Spear, F. S., 1978. Experimental calibration of the partitioning of Fe and Mg between garnet and biotite. *Contributions to Mineralogy and Petrology*, **66**, 113–117.

Field, M. T., 1975. Bedrock geology of the Ware area, central Massachusetts. *Unpubl. PhD Thesis, University of Massachusetts, Amherst.*

Fuhrman, M. L. & Lindsley, D. H., 1988. Ternary feldspar modeling and thermometry. *American Mineralogist*, **73**, 201–215.

Graham, C. M. & Powell, R., 1984. A garnet–hornblende geothermometer: calibration, testing, and application to the Pelona schist, southern California. *Journal of Metamorphic Geology*, **2**, 13–31.

Gromet, L. P., 1989. Avalonian terranes and late Paleozoic tectonism in southeastern New England: Constraints and Problems. In: *Terranes in the Circum-Atlantic Paleozoic Orogens* (ed. Dallmeyer, R. D.), *Geological Society of America Special Paper*, **230**, 193–211.

Hammarstrom, J. M. & Zen E-An, 1986. Aluminum in hornblende: an empirical igneous geobarometer. *American Mineralogist*, **71**, 1297–1313.

Hanson, R. B., 1992. Effects of fluid production on fluid flow during regional and contact metamorphism. *Journal of Metamorphic Geology*, **10**, 87–97,

Hodges, K. V. & Royden, L., 1984. Geologic thermobarometry of retrograded metamorphic rocks: an indication of the uplift trajectory of a portion of the northern Scandinavian Caledonides. *Journal of Geophysical Research*, **89**, 7077–7090.

Hodges, K. V. & Mckenna, L. W., 1987. Realistic propagation of uncertainties in geologic thermobarometry. *American Mineralogist*, **72**, 671–680.

Hyndman, R. D. & Shearer, P. M., 1989. Water in the lower continental crust: modelling magnetotelluric and seismic reflection results. *Geophysical Journal International*, **98**, 343–365.

Kerrick, D. M., 1990. *The Al_2SiO_5 polymorphs. Reviews in Mineralogy*, Vol. 22. Mineralogical Society of America.

Kohn, M. J. & Spear, F. S., 1990. Two new geobarometers for garnet amphibolites, with application to southeastern Vermont. *American Mineralogist*, **75**, 89–96.

Koziol, A. M. & Newton, R. C., 1988. Redetermination of the anorthite breakdown reaction and improvement of the plagioclase–garnet–Al_2SiO_5–quartz geobarometer. *American Mineralogist*, **73**, 216–2223.

Kozlovsky, Ye. A., 1987. *The Superdeep Hole of the Kola Peninsula*. Springer-Verlag, Berlin.

Kretz, R., 1983. Symbols for rock-forming minerals. *American Mineralogist*, **68**, 277–279.

Lacazette, A. & Engelder, T., 1992. Fluid-driven cyclic propagation of a joint in the Ithaca siltstone, Appalachian basin, New York. In: *Fault Mechanics and Transport Properties of Rocks* (eds Evans, B. & Wong, T.), pp. 297–323. International Geophysics Series, 51, Academic Press, London.

Lees, J. M. & Crowder, R. S., 1990. Tomographic imaging of local earthquake delay times for three-dimensional velocity variation in western Washington. *Journal of Geophysical Research*, **95**, 4763–4776.

Mäder, U. K. & Berman, R. G., 1991. A high pressure equation of state for carbon dioxide consistent with phase equilibrium and P–V–T data. *American Mineralogist*, **76**, 1547–1559.

Manning, C. E. & Bird, D. K., 1991. Porosity evolution and fluid flow in the basalts of the Skaergaard magma-hydrothermal system, east Greenland. *American Journal of Science,* **291,** 201–257.

Matthews, D. H. & Cheadle, M. J., 1986. Deep reflections from the Caledonides and Variscides west of Britain and comparison with the Himalayas. In: *Reflection Seismology: A Global Perspective* (eds Barazangi, M. & Brown, L.), pp. 5–19. American Geophysical Union, Geodynamics Series, 13, Washington, DC.

McMullin, D. W. A., Berman, R. G. & Greenwood, H. J., 1991. Calibration of the SGAM thermobarometer for pelitic rocks using data from phase-equilibrium experiments and natural assemblages. *Canadian Mineralogist,* **29,** 889–908.

Miyashiro, A., 1951. Kyanites in druses in kyanite–quartz veins from Saiho-ri in the Fukushinzan District, Korea. *Journal of the Geological Society of Japan,* **57,** 218–223.

Newton, R. C. & Haselton, H. T., 1981. Thermodynamics of the garnet–plagioclase–Al_2SiO_5–quartz geobarometer. In: *Thermodynamics of Minerals and Melts* (eds Newton, R. C., *et al.*), pp. 131–147. Springer-Verlag, New York.

Norton, D. L. & Knapp, R., 1977. Transport phenomena in hydrothermal systems: the nature of porosity. *American Journal of Science,* **277,** 913–936.

Nur, A. & Walder, J., 1990. Time-dependent hydraulics of the Earth's crust. In: *The Role of Fluids in Crustal Processes* (eds Bredehoeft, J. D. & Norton, D. L.), pp. 113–127. National Academy Press, Washington DC.

Oliver, N. H. S., Valenta, R. K. & Wall, V. J., 1990. The effect of heterogeneous stress and strain on metamorphic fluid flow, Mary Kathleen, Australia, and a model for large scale fluid circulation. *Journal of Metamorphic Geology,* **8,** 311–332.

Oliver, N. H. S., Cartwright, I., Wall, V. J. & Golding, S. D., 1993. The stable isotopic signature of large-scale fracture-hosted metamorphic fluid pathways, Mary Kathleen, Australia. *Journal of Metamorphic Geology,* **11,** 705–720.

Pease, M. H., 1975. Bedrock geologic map of the Stafford Springs quadrangle, Tolland County, Connecticut. *U.S. Geological Survey Open-File Report,* **75-633.**

Peper, J. D. & Pease, M. H., 1975. Geologic map of the Westford quadrangle, Connecticut. *U.S. Geological Survey Geologic Quadrangle Map,* **GQ-1214.**

Philippot, P. & Selverstone, J., 1991. Trace-element-rich brines in eclogitic veins: implications for fluid composition and transport during subduction. *Contributions to Mineralogy and Petrology,* **106,** 417–430.

Ramsay, J. G., 1980. The crack-seal mechanism of rock deformation. *Nature,* **284,** 135–139.

Robinson, P., 1978. The Bronson Hill anticlinorium and Merrimack synclinorium in central Massachusetts – an Acadian "Pennine" zone. *Geological Society of America Abstracts with Programs,* **10,** 82.

Robinson, P. & Tucker, R. D., 1982. The Merrimack synclinorium in northeastern Connecticut. *American Journal of Science,* **282,** 1735–1744.

Rodgers, J., 1981. The Merrimack synclinorium in northeastern Connecticut. *American Journal of Science,* **281,** 176–186.

Rodgers, J., 1985. Bedrock Geological Map of Connecticut. *Connecticut Geological and Natural History Survey, Department of Environmental Protection,* scale 1:125 000.

Rye, R. O., Schuiling, R. D., Rye, D. M. & Jansen, J. B. H., 1976. Carbon, hydrogen and oxygen isotope studies of the regional metamorphic complex at Naxos, Greece. *Geochimica et Cosmochimica Acta,* **40,** 1031–1049.

Schumacher, J. C., Schumacher, R. & Robinson, P., 1989. Acadian metamorphism in central Massachusetts and southwestern New Hampshire: evidence for contrasting *P–T* trajectories. In: *Evolution of Metamorphic Belts* (eds Daly, J. S., Cliff, R. A. & Yardley, B. W. D.), *Geological Society Special Publication,* **34,** 453–460.

Sibson, R. H., Robert, F. & Poulsen, K. H., 1988. High-angle reverse faults, fluid pressure cycling, and mesothermal gold quartz deposits. *Geology,* **16,** 551–555.

Sisson, V. B. & Hollister, L. S., 1990. Fluid inclusion study of pelitic schists and metamorphosed carbonate rocks, south-central Maine. *American Mineralogist,* **75,** 59–70.

Thomson, J. A., 1992. Petrology of high-grade schists, gneisses, and cordierite pegmatites in south-central Massachusetts. *Unpubl. PhD Thesis, University of Massachusetts, Amherst.*

Thomson, J. A., Peterson, V. L., Berry, H. N., IV & Barreiro, B., 1992. Recent studies in the Acadian metamorphic high, south-central Massachusetts. In: *Guidebook for Fieldtrips in the Connecticut Valley Region of Massachusetts and Adjacent States* (eds Robinson, P. & Brady, J. B.), pp. 229–255. University of Massachusetts, Department of Geology and Geography, Contribution 66.

Turner, F. J., 1981. *Metamorphic Petrology,* 2nd edn. McGraw-Hill, New York.

Vrolijk, P., 1987. Tectonically driven fluid flow in the Kodiak accretionary complex, Alaska. *Geology,* **15,** 466–469.

Walther, J. V. & Orville, P. M., 1982. Volatile production and transport in regional metamorphism. *Contributions to Mineralogy and Petrology,* **79,** 252–257.

Walther, J. V., 1990. Fluid dynamics during progressive regional metamorphism. In: *The Role of Fluids in Crustal Processes* (eds Bredehoeft, J. D. & Norton, D. L.), pp. 64–71. National Academy Press, Washington DC.

Weibel, M., 1966. *A Guide to the Minerals of Switzerland.* Interscience Publishers, London.

Williams, H., Turner, F. J. & Gilbert, C. M., 1982. *Petrography,* (2nd). Freeman, San Francisco.

Wintsch, R. P., Sutter, J. F., Kunk, M. J., Aleinikoff, J. N. & Dorais, M. J., 1992. Contrasting P–T–t paths: thermochronologic evidence for a late Paleozoic final assembly of the Avalon composite terrane in the New England Appalachians. *Tectonics,* **11,** 672–689.

Woronow, A. & Love, K. M., 1990. Quantifying and testing differences among means of compositional data suites. *Mathematical Geology,* **22,** 837–852.

Yardley, B. W. D., 1986. Fluid migration and veining in the Connemara schists, Ireland. In: *Fluid-Rock Interactions During Metamorphism* (eds Walther, J. V. & Wood, B. J.), pp. 109–131. Springer-Verlag, New York.

Received 11 April 1994; revision accepted 10 August 1994.